28. Yamamoto I, Ishii S, Usui M, Ogino T, Kaneda K. Cubitus varus deformity following supracondylar fracture of the humerus. A method for measuring rotational deformity. Clin Orthop Relat Res. 1985;201:179-85.

29. Roberts JA. Angulation of the radius in children's fractures. J Bone Joint Surg Br. 1986;68:751-4.

30. Gartland JJ Jr, Werley CW. Evaluation of healed Colles' fractures. J Bone Joint Surg Am. 1951;33:895-907.

31. Tarr RR, Garfinkel AI, Sarmiento A. The effects of angular and rotational deformities of both bones of the forearm. An in vitro study. J Bone Joint Surg Am. 1984;66:65-70.

32. Catalano LW 3rd, Cole RJ, Gelberman RH, Evanoff BA, Gilula LA, Borrelli J Jr. Displaced intra-articular fractures of the distal aspect of the radius. Long-term results in young adults after open reduction and internal fixation. J Bone Joint Surg Am. 1997;79:1290-302.

33. Lefevre-Colau MM, Babinet A, Fayad F, Fermanian J, Anract P, Roren A, Kansao J, Revel M, Poiraudeau S. Immediate mobilization compared with conventional immobilization for the impacted nonoperatively treated proximal humeral fracture. A randomized controlled trial. J Bone Joint Surg Am. 2007;89:2582-90.

34. O'Driscoll SW, Spinner RJ, McKee MD, Kibler WB, Hastings H 2nd, Morrey BF, Kato H, Takayama S, Imatani J, Toh S, Graham HK. Tardy posterolateral rotatory instability of the elbow due to cubitus varus. J Bone Joint Surg Am. 2001;83:1358-69.

35. Schemitsch EH, Richards RR. The effect of malunion on functional outcome after plate fixation of fractures of both bones of the forearm in adults. J Bone Joint Surg Am. 1992;74:1068-78.

36. Trousdale RT, Linscheid RL. Operative treatment of malunited fractures of the forearm. J Bone Joint Surg Am. 1995;77:894-902.

37. Rieger M, Gabl M, Gruber H, Jaschke WR, Mallouhi A. CT virtual reality in the preoperative workup of malunited distal radius fractures: preliminary results. Eur Radiol. 2005;15:792-7.

38. Athwal GS, Ellis RE, Small CF, Pichora DR. Computer-assisted distal radius osteotomy. J Hand Surg [Am]. 2003;28:951-8.

39. Dumont CE, Thalmann R, Macy JC. The effect of rotational malunion of the radius and the ulna on supination and pronation. J Bone Joint Surg Br. 2002;84:1070-4.

40. Chapman MW, Gordon JE, Zissimos AG. Compression-plate fixation of acute fractures of the diaphyses of the radius and ulna. J Bone Joint Surg Am. 1989;71:159-69.

41. Chung MS, Baek GH. Three-dimensional corrective osteotomy for cubitus varus in adults. J Shoulder Elbow Surg. 2003;12:472-5.

42. Bellemore MC, Barrett IR, Middleton RW, Scougall JS, Whiteway DW. Supracondylar osteotomy of the humerus for correction of cubitus varus. J Bone Joint Surg Br. 1984;66:566-72.

43. Graham B, Tredwell SJ, Beauchamp RD, Bell HM. Supracondylar osteotomy of the humerus for correction of cubitus varus. J Pediatr Orthop. 1990;10:228-31.

44. Abe M, Ishizu T, Nagaoka T, Onomura T. Recurrent posterior dislocation of the head of the radius in post-traumatic cubitus varus. J Bone Joint Surg Br. 1995;77:582-5.

45. Abe M, Ishizu T, Shirai H, Okamoto M, Onomura T. Tardy ulnar nerve palsy caused by cubitus varus deformity. J Hand Surg [Am]. 1995;20:5-9.

46. Spinner RJ, O'Driscoll SW, Davids JR, Goldner RD. Cubitus varus associated with dislocation of both the medial portion of the triceps and the ulnar nerve. J Hand Surg [Am]. 1999;24:718-26.

47. Mahaisavariya B, Laupattarakasem W. Supracondylar fracture of the humerus: malrotation versus cubitus varus deformity. Injury. 1993;24:416-8.

48. Laupattarakasem W, Mahaisavariya B, Kowsuwon W, Saengnipanthkul S. Pentalateral osteotomy for cubitus varus. Clinical experiences of a new technique. J Bone Joint Surg Br. 1989;71:667-70.

49. Fernandez DL. Correction of post-traumatic wrist deformity in adults by osteotomy, bone-grafting, and internal fixation. J Bone Joint Surg Am. 1982;64:1164-78.

50. Fernandez DL. Radial osteotomy and Bowers arthroplasty for malunited fractures of the distal end of the radius. J Bone Joint Surg Am. 1988;70:1538-51.

51. Posner MA, Ambrose L. Malunited Colles' fractures: correction with a biplanar closing wedge osteotomy. J Hand Surg [Am]. 1991;16:1017-26.

52. Shea K, Fernandez DL, Jupiter JB, Martin C Jr. Corrective osteotomy for malunited, volarly displaced fractures of the distal end of the radius. J Bone Joint Surg Am. 1997;79:1816-26.

53. Zdravkovic V, Bilic R. Computer-assisted preoperative planning (CAPP) in orthopaedic surgery. Comput Methods Programs Biomed. 1990;32:141-6.

54. Malone KJ, Magnell TD, Freeman DC, Boyer MI, Placzek JD. Surgical correction of dorsally angulated distal radius malunions with fixed angle volar plating: a case series. J Hand Surg [Am]. 2006;31:366-72.

55. Bonel HM, Jager L, Frei KA, Galiano S, Srivastav SK, Flohr T, Reiser MF, Dinkel HP. Optimization of MDCT of the wrist to achieve diagnostic image quality with minimum radiation exposure. AJR Am J Roentgenol. 2005;185:647-54.

SCIENTIFIC ARTICLE

Relationship Between the Fracture Location and the Kinematic Pattern in Scaphoid Nonunion

Hisao Moritomo, MD, PhD, Tsuyoshi Murase, MD, PhD, Kunihiro Oka, MD, PhD, Hiroyuki Tanaka, MD, PhD, Hideki Yoshikawa, MD, PhD, Kazuomi Sugamoto, MD, PhD

Purpose The purpose of this study was to obtain 3-dimensional and quantitative information regarding the pathological kinematics of the wrist with scaphoid nonunion using an *in vivo* and 3-dimensional motion analysis. We specifically tested the hypothesis that the fracture location is related to the kinematic pattern.

Methods We studied wrist kinematics during wrist flexion-extension motion and radioulnar deviation in 13 patients with scaphoid nonunion, using a markerless bone registration technique. Magnetic resonance images or computed tomography (CT) images of the wrist were acquired with the wrist in the neutral and 4 extreme positions of flexion, extension, radial deviation, and ulnar deviation. Three-dimensional animations were created of the carpal motions and interfragmentary motions between the distal and proximal fragments of the scaphoid. Based on the fracture location, accurate estimates of the relative positions and orientations of the carpal bones were analyzed.

Results There were 2 clear patterns of the interfragmentary motions of the scaphoid based on the fracture location. In the mobile type scaphoid nonunion (7 cases), the fracture was located distal to the apex of the scaphoid dorsal ridge (scaphoid apex), and the distal scaphoid was unstable relative to the proximal scaphoid. The distal fragment showed a "book-opening" motion from wrist flexion to extension. In the stable type scaphoid nonunion (6 cases), the fracture was located proximal to the scaphoid apex, and the interfragmentary motion was considerably less than with the distal type.

Conclusions Carpal instability following scaphoid nonunion appears to be related to whether the fracture line passes distal or proximal to the scaphoid apex, where the dorsal scapholunate interosseous ligament and the dorsal intercarpal ligament attach. Three-dimensional imaging should be considered when assessing scaphoid nonunions to identify the exact location of the fracture. This may allow the clinician to choose the best treatment option. *(J Hand Surg 2008;33A:1459–1468.*

Key words Biomechanics, instability, scaphoid nonunion, 3-dimensional motion analysis, wrist.

From the Department of Orthopaedics, Osaka University, Osaka, Japan.

The authors would like to acknowledge assistance during parts of the experimental procedures from Sayuri Arimitsu, MD, Department of Orthopaedics, Osaka University; Ryoji Nakao, computer programmer, Department of Orthopaedics, Osaka University; Kakuro Denno, MD, Department of Orthopaedics, Kansai Rosai Hospital; Kenji Miki, MD, Department of Orthopaedics, Amagasaki Chuou Hospital; and Mitsuru Horiki, MD, Department of Orthopaedics, Kansai Rosai Hospital.

Received for publication November 30, 2007; accepted in revised form May 29, 2008.

This study was supported in part by Grants-in-Aid for Scientific Research, the Ministry of Education, Science, and Culture of Japan.

No benefits in any form have been received or will be received related directly or indirectly to the subject of this article.

Corresponding author: Hisao Moritomo, MD, PhD, Department of Orthopaedics, Osaka University, 2-2 Yamadaoka, Suita-shi, Osaka, 565-0871 Japan; e-mail: moritomo@ort.med.osaka-u.ac.jp.

0363-5023/08/33A09-0001$34.00/0
doi:10.1016/j.jhsa.2008.05.035

THE SCAPHOID FUNCTIONS as a complex link between the proximal and distal carpal rows of the wrist.[1] The scaphoid plays an important role in wrist function; thus, scaphoid fracture nonunion changes wrist mechanics, which can lead to carpal instability and secondary degenerative changes. Although there have been a few reported factors that are responsible for carpal instability after scaphoid fracture, such as fracture location[2–4] and lunate morphology,[5] the exact mechanism of instability is still unknown.

The carpal displacements caused by scaphoid nonunion have been analyzed using 3-dimensional reconstruction of CT with the wrist in the neutral position. Two distinct offset patterns of the distal fragment with respect to the proximal fragment have been identified:[2–4] a volar type, in which the distal fragment overhangs palmarly relative to the proximal fragment; and a dorsal type, in which the distal fragment shifts dorsally relative to the proximal fragment. The volar types of scaphoid nonunion have been found to occur exclusively after fractures distal to the apex of the dorsal ridge of the scaphoid (scaphoid apex, Fig. 1), and the dorsal types have been associated with fractures proximal to the scaphoid apex.[3,4]

The nature and magnitude of the interfragmentary motion that is present in scaphoid nonunion and its kinematic effects on the remainder of the wrist are poorly understood. An *in vitro* kinematic study of the wrist after scaphoid waist osteotomy in cadavers[6] found that the distal scaphoid assumed a relatively flexed stance and had increased motion, while the proximal scaphoid and lunate assumed a relatively extended stance and had less motion. However, such *in vitro* experiments cannot completely reproduce the physical muscular force that is exerted across the wrist *in vivo*. These limitations could alter carpal motion kinematics. Recently, researchers have been able to measure the *in vivo* kinematics of the human joint using noninvasive techniques.[7–10] Such *in vivo* research may provide more accurate information about the kinematics of scaphoid nonunion.

A few *in vitro* studies have dealt with the biomechanical consequences of scaphoid fractures on wrist kinematics[6] and load distribution;[11] however, the findings have not been confirmed *in vivo*. Furthermore, it is unknown whether fracture location determines the kinematic effects that these fractures have on the remainder of the wrist. Thus, this study was designed to obtain 3-dimensional and quantitative data regarding the pathological kinematics of the wrist following scaphoid nonunion, using *in vivo* motion analysis. We specifically tested the hypothesis that the fracture location with respect to the scaphoid apex is related to the kinematic pattern.

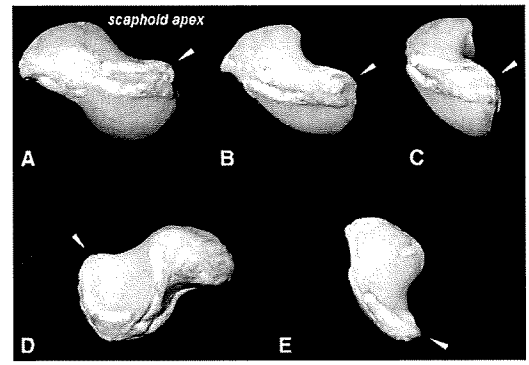

FIGURE 1: The scaphoid apex is the most dorsal and ulnar nonarticulating part of the scaphoid. The scaphoid of a right cadaver wrist seen from the **A** radial, **B** radiodorsal, **C** dorsal, **D** ulnar, and **E** distal side. The location of the *scaphoid apex* on the dorsal ridge is indicated by an arrow head.

MATERIALS AND METHODS

We studied the *in vivo* kinematics of the wrist joint during wrist flexion-extension motion and radioulnar deviation in 13 patients with scaphoid nonunion (10 men and 3 women; age range, 19–57 years; mean age, 29 years, Table 1). All patients provided their written informed consent before being enrolled in the study.

Fracture location

In order to identify the location of the scaphoid apex, we took CT scans of both wrists in the wrist neutral position for all patients, using a clinical helical type scanner (Lightspeed Ultra16, General Electric, Maukesha, WI) with a slice thickness of 0.635 mm. We determined the neutral wrist position by aligning the third metacarpal with the dorsal surface of the forearm. First, the scaphoid apex was carefully identified using the 3-dimensional image of the scaphoid, reconstructed from the CT data. The scaphoid apex is the most dorsal and ulnar nonarticulating part of the scaphoid, which is determined only by osseous geometry. The scaphoid apex can be seen from various points of view in 3-dimensional imaging (Fig. 1). Usually, to identify the scaphoid apex, the radiodorsal view is the best. Comparing it to the 3-dimensional image of the contralateral scaphoid is helpful, especially when the osteophytes exist around the fracture site. Next, the orientation of the fracture line relative to the scaphoid apex was identified on 3-dimensional imaging. The straight-line distance between the scaphoid apex and a point at which the fracture line crossed the dorsoulnar cortex of the

TABLE 1. Patient Data

Type of Scaphoid Nonunion	Case	Fracture Type: Herbert Classification	Fracture Type: Garcia-Elias Classification	Fracture Type: Our Classification	Age (Years)	Gender	Duration of Nonunion (Months)	Apex-Fracture Distance (mm)*	Radiolunate Angle (°)†	DISI Deformity	Degenerative Change
Mobile type	1	B1		Type 2	27	M	6	9.0	12	Present	Absent
	2	B1		Type 2	23	M	2	7.8	25	Present	Absent
	3	B2			20	M	33	12.9	5	Present	Absent
	4	B2			39	M	480	8.5	42	Present	Radioscaphoid joint
	5	B5			21	F	2	11.2	39	Present	Absent
	6	B3	Type 2		34	M	5	7.7	19	Present	Absent
	7	B3	Type 2		25	M	52	7.1	14	Present	Absent
	Average				**27**		**83**	**9.2**	**22**		
	SD				7		176	**2.1**	**14**		
Stable type	8	B1		Type 1	34	M	205	5.4	−10	Absent	Radioscaphoid joint
	9	B1		Type 1	19	M	9	3.1	−10	Absent	Absent
	10	B3	Type 1		26	F	11	2.4	−5	Absent	Absent
	11	B3	Type 1		26	F	48	4.5	−3	Absent	Absent
	12	B3	Type 1		57	M	7	3.7	−5	Absent	Radioscaphoid joint
	13	B3	Type 1		19	M	33	7.5	−5	Absent	Absent
	Average				**30**		**52**	**4.4**	**−6**		
	SD				**14**		**77**	**1.8**	**3**		
Total	**Average**				**28**		**69**	**7.0**	**9**		
	SD				**11**		**135**	**3.1**	**18**		

DISI, dorsal intercaleted segment instability.
*The straight line distance between the scaphoid apex and fracture line. All the fracture location in the type 2 scaphoid nonunion is distal to the scaphoid apex.
†When the lunate rotated dorsally, the radiolunate angle is shown as a minus value.

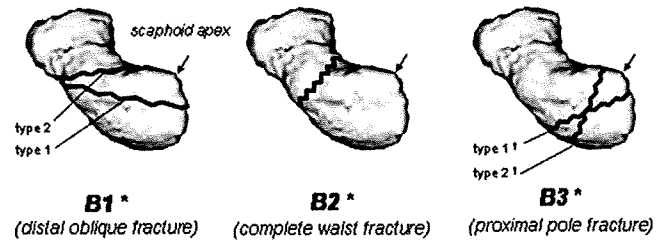

mobile type nonunion	stable type nonunion
• type 2 B1 • B2 • type 2 B3 • B5	• type 1 B1 • type 1 B3

FIGURE 2: New classification system of the scaphoid fracture based on the relationship between fracture location and the scaphoid apex. The right scaphoids are seen from the radiodorsal side. *According to Herbert's classification system of scaphoid fractures. †According to the classification system of proximal pole fractures by Garcia-Elias.

scaphoid (apex-fracture distance) was measured using specially developed software (Orthopedics Viewer, Osaka University, Osaka, Japan).

The fracture pattern was first classified based on the fracture location, using the Herbert classification system[12] (Fig. 2). There were 4 cases of B1 (distal oblique fracture), 2 cases of B2 (waist fracture), 6 cases of B3 (proximal pole fracture), and 1 case of B5 (comminuted waist fracture). The B3 cases were further classified according to the Garcia-Elias classification system.[13] Among the B3 group, there were 4 cases of type 1, where the fracture line runs proximal to the scaphoid apex, and 2 cases of type 2, where the fracture line runs distal to the scaphoid apex. We also classified the B1 cases based on the dorsal portion of the fracture relative to the scaphoid apex. Among the B1 group, there were 2 type 1 cases, where the fracture line runs proximal to the scaphoid apex, and 2 type 2 cases, where the fracture line runs distal to the scaphoid apex.

Motion analysis

In order to obtain the kinematic data (not to identify the scaphoid apex or fracture line), we used magnetic resonance imaging (4 cases) or CT (9 cases) of the wrist in 5 positions (the neutral and 4 extreme positions of flexion, extension, radial deviation, and ulnar deviation). Our kinematic analysis technique and its accuracy have been documented previously.[7] Magnetic resonance image data of the wrists were obtained using a 1.5-T commercial magnetic resonance system (Magnetom Vision PlusR 1.5-T MRI; Siemens AG, Erlangen, Germany) in conjunction with a receive-only body-array surface coil. We used a 3-dimensional sequence (3-dimensional fast low angle shot) with a repetition time of 2.3 ms, an echo time of 33 ms, a flip angle of 45°, a 160-mm field of view, and a 0.5-mm thickness, on a contiguous slice with a pixel size of 0.6 × 0.8 mm. Computed tomography images were obtained using the same technique described earlier. To immobilize the elbow and the wrist, a special positioning device was used. This device has a grip bar and has 3 motion axes that all cross perpendicularly at the wrist joint and enable the wrist to move along any specific plane. The contours of each bone were mapped from the volume images and 3-dimensional surface models of the bones were constructed. The kinematic variables were calculated by registering the bone in 1 position and then comparing the data with those of other positions. The volume registration technique[7] was used in this study. The data for all left wrists were mathematically converted into right wrist data.

The radius and all the carpal bones except the pisiform were registered, and the relative motion of each bone was calculated. The proximal and distal fragments of the scaphoid were tracked as separate carpal bones. Three-dimensional animations of carpal motion and the interfragmentary motion that occurred between the distal and proximal fragments of the scaphoid were created using originally developed software (Orthopedics Viewer, Osaka University, Osaka, Japan).

Accurate estimates of the relative positions and orientations of the bones during flexion-extension motion and radioulnar deviation were obtained using Euler angles. Euler angles describe the angular motion of a body in 3-dimensional space. In this application, the Euler angles are presented as the roll-pitch-yaw angle of the carpal bones relative to the radius. For the interfragmentary motion, the roll-pitch-yaw angle of the distal scaphoid relative to the proximal scaphoid in the wrist neutral position was used.

During wrist flexion-extension motion and radioulnar deviation, the contribution rates of the motion between the radius and distal scaphoid, the motion between the radius and proximal scaphoid, and the radiolunate motion to global wrist motion were studied. Two data points of the extreme positions for each motion plane were obtained. The radiocapitate motion was used as a global wrist motion.[8] The contribution

data in this study were compared with a database of normal wrists obtained in the previous study.[7]

The coordinate system was constructed according to the International Society of Biomechanics (http://www.isbweb.org/standards/wrist.html) definition: the origin is located midway between the distal radius at the level of the ridge between the radioscaphoid fossa and the radiolunate fossa. The Z axis is the axis of flexion and extension; the Y axis is the axis of pronation and supination; and the X axis is the axis of radial and ulnar deviation. The Y axis is the line parallel to the long shaft of the radius that intersects with the origin. The Z axis is the line perpendicular to the Y axis and in a plane defined by the tip of the radial styloid, the base of the concavity of the sigmoid notch, and the specified origin. The X axis is defined as the common line perpendicular to both the Y and Z axes.

All data are expressed as means ± SD. Statistical analysis of differences was performed using Student's *t*-test; $p<.05$ was considered significant.

RESULTS

Two clearly separate patterns of interfragmentary motions of the scaphoid and other carpal motions were identified: the *mobile* type scaphoid nonunion (7 cases) and the *stable* type scaphoid nonunion (6 cases) (Table 1). In the mobile type, the dorsal portion of the fracture was always distal to the scaphoid apex. The fracture types in this group were B1 type 2, B2, B3 type 2, and B5 (Fig. 2). The average apex-fracture distance was 9 mm (range, 7–13 mm). In the stable type, the dorsal portion of the fracture was always proximal to the scaphoid apex. The fracture types in this group were B1 type 1 and B3 type 1 (Fig. 2). The average apex-fracture distance was 4 mm (range, 2–8 mm). In the wrist neutral position, all patients with a mobile type scaphoid nonunion had an extended stance of the lunate or a dorsal intercalated segment instability (DISI) deformity, in which the radiographic radiolunate angle was 22° ± 14°. The radiolunate angle was −6° ± 3° in the stable type nonunion; none of the patients with stable type nonunion had a DISI deformity (Table 1).

Motion of the mobile type scaphoid nonunion

In the animation of wrist flexion-extension motion during which the proximal scaphoid was fixed and the other bones were moving, the distal fragment showed a "book-closing" motion during wrist flexion (the distal scaphoid rotates palmarly, and there is some overlap of the proximal and distal scaphoid segments in the sagittal view) and a "book-opening" motion during wrist extension (the distal scaphoid extends, resulting in a palmarly opening bone defect) (Fig. 3A). The distal scaphoid flexed 7° ± 10° and extended 24° ± 15° relative to the proximal scaphoid during motion from the neutral position to wrist flexion and from the neutral position to wrist extension, respectively (Table 2). The scaphoid nonunions categorized as B1 type 2 (oblique fracture, cases 1 and 2) and B3 type 2 (proximal pole fracture, cases 6 and 7, Fig. 4) were unstable during the flexion-extension motion and behaved identically to B2 (waist fracture, cases 3 and 4). The interfragmentary rotations in radioulnar deviation were much smaller than in flexion-extension motion, where the distal scaphoid flexed 0° ± 4° and extended 0° ± 12°relative to the proximal scaphoid with wrist radial deviation and ulnar deviation, respectively (Table 2). In the animation, however, the distal scaphoid appeared to impinge with the radial styloid in wrist radial deviation in all cases (Fig. 3B).

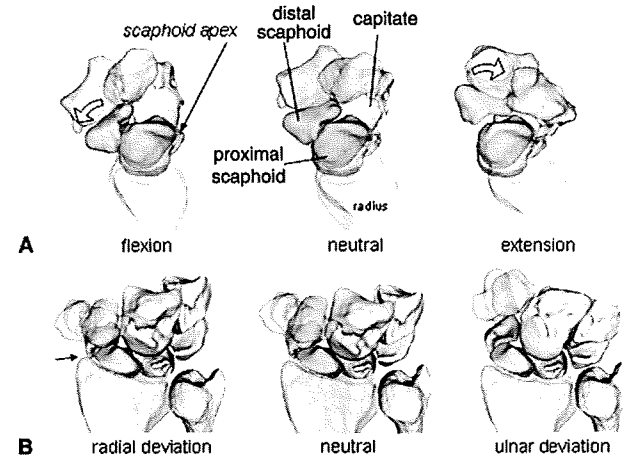

FIGURE 3: Motions of the mobile type waist nonunion (B2, case 4). **A** Radial views during wrist flexion–extension motion. The distal fragment shows a "book-closing" motion during wrist flexion and a "book-opening" motion during wrist extension. **B** Dorsal views during radioulnar deviation. Note the impingement between the distal scaphoid and the radial styloid in radial deviation (arrow). The proximal scaphoid is fixed, and the other bones are moving. (Videos can be viewed on the *Journal's* Web site, www.jhandsurg.org.)

The rotation contribution rates of the motion between the radius and distal scaphoid, the motion between the radius and proximal scaphoid, and the radiolunate motion to global wrist motion were 87%, 54%, and 39% during wrist flexion-extension, and 32%, 31%, and 1% during wrist radioulnar deviation, respectively (Table 3). The rotation contribution rates of the scaphoid and the lunate from a database of normal wrists were 82% and 56% during wrist flexion-extension, and 36%, and 37% during wrist radioulnar deviation, re-

TABLE 2. Euler Angles of Carpal Motion

Global Wrist Motion	Flexion (°)			Extension (°)			Radial Deviation (°)			Ulnar Deviation (°)		
Bone	Z	Y	X	Z	Y	X	Z	Y	X	Z	Y	X
Mobile type												
Distal scaphoid to proximal scaphoid	7 ± 10	−2 ± 2	4 ± 4	−24 ± 15	−3 ± 4	−3 ± 5	0 ± 4	−1 ± 4	1 ± 3	0 ± 12	1 ± 3	1 ± 5
Distal scaphoid to radius	40 ± 9	0 ± 5	3 ± 8	−37 ± 15	0 ± 6	0 ± 7	2 ± 10	−3 ± 5	−4 ± 7	−5 ± 17	4 ± 3	9 ± 4
Proximal scaphoid to radius	33 ± 11	2 ± 5	−1 ± 6	−13 ± 9	3 ± 4	3 ± 4	2 ± 8	−1 ± 4	−5 ± 5	−5 ± 9	3 ± 4	9 ± 5
Lunate to radius	26 ± 12	1 ± 4	−2 ± 6	−9 ± 5	1 ± 2	2 ± 6	6 ± 7	0 ± 3	−7 ± 9	−6 ± 11	1 ± 3	10 ± 7
Capitate to radius	46 ± 12	3 ± 4	1 ± 12	−43 ± 19	3 ± 5	2 ± 9	−3 ± 12	−3 ± 7	−14 ± 11	10 ± 17	−2 ± 8	29 ± 13
Stable type												
Distal scaphoid to proximal scaphoid	1 ± 8	0 ± 6	1 ± 5	−7 ± 5	−1 ± 3	0 ± 1	5 ± 5	1 ± 3	−2 ± 4	3 ± 7	1 ± 5	1 ± 4
Distal scaphoid to radius	34 ± 10	2 ± 5	3 ± 6	−23 ± 9	−6 ± 6	2 ± 2	12 ± 8	−1 ± 5	−4 ± 5	−2 ± 12	0 ± 1	13 ± 7
Proximal scaphoid to radius	33 ± 10	2 ± 4	2 ± 6	−18 ± 12	−5 ± 5	2 ± 2	8 ± 6	−2 ± 5	−3 ± 4	−5 ± 6	0 ± 5	11 ± 6
Lunate to radius	23 ± 8	2 ± 6	3 ± 6	−10 ± 7	−4 ± 4	1 ± 5	10 ± 6	−1 ± 4	0 ± 5	−5 ± 9	0 ± 1	12 ± 5
Capitate to radius	42 ± 18	2 ± 4	4 ± 12	−33 ± 16	−7 ± 9	2 ± 10	9 ± 15	−5 ± 5	−18 ± 9	12 ± 11	−1 ± 5	24 ± 10

Z, + flexion, − extension; Y, + pronation, − supination; X, + ulnar deviation, − radial deviation

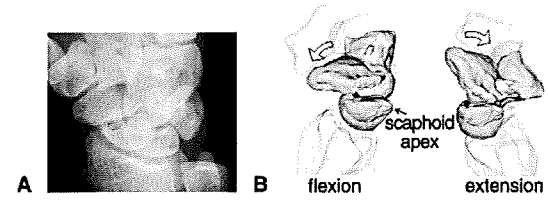

FIGURE 4: The mobile type proximal pole nonunion (B3 type 2, case 7). **A** The semipronated view of the plain radiograph does not show clear relationship between the fracture line and the scaphoid apex. **B** Three-dimensional animation shows a marked interfragmentary motion during flexion–extension motion. The proximal scaphoid is fixed, and the other bones are moving (these videos can be viewed at the *Journal's* Web site, www.jhandsurg.org).

spectively (as previously published[7]). There was a relative decrease in contribution rates of the motion between the radius and proximal scaphoid ($p<.001$) and the radiolunate motion ($p<.001$) during wrist flexion-extension and of the radiolunate motion during wrist radioulnar deviation ($p<.001$) when compared to the normal wrist.

Motion of the stable type scaphoid nonunion

The interfragmentary motion with the stable type scaphoid nonunion during wrist flexion-extension motion was significantly smaller than that with the mobile type ($p<.05$, Fig. 5A), in which the distal scaphoid flexed 1° ± 8° and extended 7° ± 5°relative to the proximal scaphoid in wrist flexion and extension, respectively (Table 2). The interfragmentary motions in radioulnar deviation were also small (Fig. 5B), but there was not a significant difference with the mobile type. The distal scaphoid flexed 5° ± 5° and extended 3° ± 7° relative to the proximal scaphoid in wrist radial deviation and ulnar deviation, respectively (Table 2).

The rotation contribution rates of the motion between the radius and distal scaphoid, the motion between the radius and proximal scaphoid, and the radiolunate motion to global wrist motion were 79%, 68%, and 44% during wrist flexion-extension and 42%, 34%, and 30% during wrist radioulnar deviation, respectively (Table 3). There was a relative decrease in contribution rates of the motion between the radius and proximal scaphoid ($p<.005$) and the radiolunate motion ($p<.01$) during wrist flexion-extension when compared to normal wrists (82% and 56%, respectively).[7] There were no significant differences in contribution rates during wrist radioulnar deviation. When compared to the mobile type, there was a relative decrease in contribution rates of the motion between the radius and the distal scaphoid during wrist flexion-extension ($p<.05$) and a relative increase in contribution rates of the radiolunate motion during wrist radioulnar deviation ($p<.005$).

There was no significant relationship between the interfragmentary motion and the duration (number of months) of the nonunion or between the interfragmentary motion and degenerative changes in the mobile type and the stable type.

DISCUSSION

A few *in vitro* studies[6,11] have investigated the biomechanical consequences of scaphoid fractures; however, the findings have never been confirmed *in vivo*. Furthermore, the relationship between the fracture location and the nature and magnitude of the interfragmentary motion of the scaphoid and its kinematic effects on the reminder of the wrist are still unknown. Therefore, we designed this study to investigate the pathological kinematics of the wrist with scaphoid nonunion in terms of the fracture location using *in vivo* 3-dimensional motion analysis.

The kinematic technique used in this study has some limitations. The primary disadvantage is that this study is based on static 3-dimensional views of the carpus in a limited number of wrist positions. Static measurement does not include any inertial or functional effects that might occur during normal wrist motion. This study was conducted with only 13 patients, which results in a low power analysis. For the motion analysis, we used magnetic resonance images in 4 cases and CT in 9 cases. Although accuracy of motion analysis using magnetic resonance images has been proved previously, uniform protocol would have been more valuable. However, CT data were used in all patients regarding fracture location, and this kinematic technique allows 3-dimensional data to be collected *in vivo* and pathological kinematics to be studied noninvasively.

In previous studies dealing with 3-dimensional deformity of scaphoid nonunion at the wrist neutral position,[3,4] it was found that a humpback deformity of the scaphoid and a DISI deformity predominantly occurred following fractures in which the dorsal portions were located distal to the scaphoid apex; the deformities were less commonly associated with fractures located proximal to the apex. It was suggested that fractures distal to the insertion of the proximal fiber of the dorsal intercarpal ligament and the dorsal scapholunate interosseous ligament are destabilized and that this allows the distal fragment to flex and the proximal fragment to extend. Conversely, in proximally located fractures, the ligamentous restraints are still attached to the distal fragment

TABLE 3. Rotation Contribution Rates of the Scaphoid and Lunate Motions Respective to the Radius to Global Wrist Motion

	Mobile Type				Stable Type				Normal[6]	
	Case	Distal Scaphoid (%)	Proximal Scaphoid (%)	Lunate (%)	Case	Distal Scaphoid (%)	Proximal Scaphoid (%)	Lunate (%)	Scaphoid (%)	Lunate (%)
Flexion–extension motion	1	89	43	32	8	79	69	50		
	2	88	60	49	9	83	57	47		
	3	94	77	44	10	79	77	51		
	4	87	23	29	11	72	83	38		
	5	73	62	49	12	92	54	38		
	6	93	69	40	13	68	69	42		
	7	81	43	31						
Average		87	54	39		79	68	44	81.7	56.4
SD		7	19	9		8	11	6		
Radioulnar deviation	1	27	28	−1	8	68	66	54		
	2	51	49	2	9	29	18	27		
	3	44	45	0	10	38	41	43		
	4	21	13	8	11	47	40	45		
	5	21	14	7	12	33	11	0		
	6	31	36	−5	13	37	29	10		
	7	30	35	−4						
Average		32	31	1		42	34	30	36.0	36.8
SD		11	14	5		14	20	21		

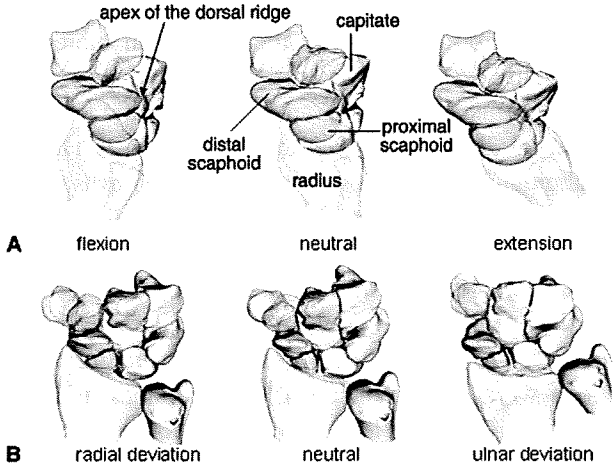

FIGURE 5: Motions of the stable type proximal pole nonunion (B3 type 1, case 10). The interfragmentary motions were small during both **A** the flexion-extension motion and **B** the radioulnar deviation. The proximal scaphoid is fixed, and the other bones are moving (these videos can be viewed at the *Journal's* Web site, www.jhandsurg.org).

and offer additional stability. This explains why the distal or volar type of nonunion is consistently associated with a DISI type of carpal malalignment.

In the current *in vivo* motion analysis, there were clearly 2 patterns of interfragmentary motions based on the fracture location. When the fracture was located distal to the scaphoid apex, the distal scaphoid was unstable relative to the proximal scaphoid (mobile type). The distal fragment showed a "book-opening" motion during motion from wrist flexion to extension. In contrast, when the fracture was located proximal to the apex, the amount of interfragmentary motion was significantly less than with the mobile type nonunion (stable type). In the mobile type, there was an uncoupling of the proximal and distal fragments, resulting in both abnormal kinematics and load distribution. Furthermore, the animations in the mobile type showed that the intercalated segment is no longer synchronized with the distal row by way of the scaphoid; the distal scaphoid fragment functionally becomes part of the distal row, and the proximal

scaphoid fragment is incorporated within the proximal row.

In patients with the B1 fracture (distal oblique fracture) and the B3 fracture (proximal pole fracture), there was a spectrum of fracture location as the fracture line runs close to the scaphoid apex. Regarding the B3 fracture, Garcia-Elias et al.[13] classified the proximal pole nonunion into type 1, where the fracture line runs proximal to the dorsal scapholunate interosseous ligament, and type 2, where the fracture line runs distal to the dorsal scapholunate interosseous ligament (Fig. 2). We confirmed that the kinematic patterns of type 1 and type 2 proximal pole nonunions were different; type 2 proximal pole nonunions were unstable and behaved identically to scaphoid waist nonunion (Fig. 4). Therefore, the natural history of type 2 nonunions should be different from that of type 1. In type 2, even though the fracture is located at the proximal pole, the bone defect is relatively large, and the patient will develop a DISI deformity and carpal instability. The proximal fragment usually has a capsular attachment at its dorsal aspect and a strong ligamentous connection with the lunate, which thus maintains some blood supply. Type 1 fractures essentially do not alter the equilibrium of forces between the scaphoid and the lunate. Because wrist stability is not at risk, the bone defect should be smaller, and the patient should have fewer symptoms. However, necrosis of the proximal fragment can easily occur due to the poor vascularity.

We classified B1 fractures (distal oblique fracture) into type 1, where the fracture line runs proximal to the scaphoid apex, and type 2, where the fracture line runs distal to the scaphoid apex (Fig. 2). The similar kinematic pattern as the proximal pole nonunion between type 1 and type 2 was found in the B1 oblique nonunions. We consider that the natural history of B1 type 2 nonunion should be different from B1 type 1 nonunion. However, further investigation is required to ascertain this theory because sample size in this study was indeed small.

Analysis for the rotation contribution rates revealed that there was a relative decrease in the motion between the radius and proximal scaphoid and the radiolunate motion in scaphoid nonunion when compared to the normal wrists. When a comparison was made between the mobile type and the stable type, however, there was no significant difference in contributions of the proximal scaphoid and the lunate. These results suggest that even stable scaphoid nonunion considerably affects radiocarpal kinematics. In contrast, the function of the midcarpal joint was relatively well preserved. This may explain why degenerative change following scaphoid nonunion starts from the radiocarpal joint.

There was no significant relationship between the interfragmentary motion and the duration (number of months) of the nonunion in this study. However, we can assume that the mobile nonunion would deteriorate more rapidly than the stable type nonunion and that the stable type nonunion would have a more chronic nature. We believe that the reason our results did not show a significant difference was due to the small number of the patients. On the other hand, it has been reported that a longstanding proximal third scaphoid nonunion can change the shape of the proximal fragment and develop a DISI deformity and severe degenerative changes.[14] Therefore, we also speculate that a longstanding nonunion of the stable type nonunion and resultant arthritis would change the kinematics within the scaphoid.

There is room for argument on other factors that may influence the stability on scaphoid nonunions, such as the mechanism of injury and the anatomic variance of the dorsal intercarpal ligament, which is controversial with respect to its insertion.[15] Moreover, Haase et al. reported that type 2 lunate morphology was associated with significantly decreased incidence of DISI deformity.[5] They theorized that the type 2 lunate's added articulation with the hamate lends some additional stability that resists abnormal extension of the lunate. They also found there was no association between lunate morphology and fracture location (proximal pole or waist). However, they did not classify their waist scaphoid fractures into subtypes, and it seems that their waist fracture group includes both Herbert B1 (distal oblique fracture) and B2 (waist fracture). It is possible that more exact classification of fracture location would clarify a more detailed relationship between lunate morphology, fracture location, and instability.

We found that the pattern of abnormal kinematics that occurs following scaphoid nonunion depends predominantly on whether the dorsal portion of the fracture line passes distal or proximal to the scaphoid apex. This study suggests that to identify the exact location of the fracture using 3-dimensional imaging is helpful in planning surgical tactics for the treatment of scaphoid nonunions. We hope this study raises concern regarding the scaphoid apex as a critical anatomic point in scaphoid nonunion pathology.

REFERENCES

1. Patterson RM, Moritomo H, Yamaguchi S, Viegas SF. Scaphoid anatomy and mechanics: update and review. Atlas Hand Clin 2004; 9:129–140.
2. Nakamura R, Imaeda T, Horii E, Miura T, Hayakawa N. Analysis of

scaphoid fracture displacement by three-dimensional computed tomography. J Hand Surg 1991;16A:485–492.
3. Moritomo H, Viegas SF, Elder KW, Nakamura K, DaSilva MF, Boyd NL, et al. Scaphoid nonunions: A 3-dimensional analysis of patterns of deformity. J Hand Surg 2000;25A:520–528.
4. Oka K, Moritomo H, Murase T, Goto A, Sugamoto K, Yoshikawa H. Patterns of carpal deformity in scaphoid nonunion: a 3-dimensional and quantitative analysis. J Hand Surg 2005;30A:1136–1144.
5. Haase SC, Berger RA, Shin AY. Association between lunate morphology and carpal collapse patterns in scaphoid nonunions. J Hand Surg 2007;32A:1009–1012.
6. Smith DK, Cooney WP III, An KN, Linscheid RL, Chao EYS. The effects of simulated unstable scaphoid fracture on carpal motion. J Hand Surg 1989;14A: 283–291.
7. Goto A, Moritomo H, Murase T, Oka K, Sugamoto K, Arimura T, et al. In vivo three-dimensional wrist motion analysis using magnetic resonance imaging and volume-based registration. J Orthop Res 2005;23:750–756.
8. Neu CP, Crisco JJ, Wolfe SW. In vivo kinematic behavior of the radio-capitate joint during wrist flexion-extension and radio-ulnar deviation. J Biomech 2001;34:1429–1438.
9. Moritomo H, Murase T, Goto A, Oka K, Sugamoto K, Yoshikawa H. In vivo, 3-dimensional kinematics of the midcarpal joint of the wrist. J Bone Joint Surg 2006;88A:611–621.
10. Crisco JJ, Coburn JC, Moore DC, Akelman E, Weiss AP, Wolfe SW. In vivo radiocarpal kinematics and the dart thrower's motion. J Bone Joint Surg 2005;87A:2729–2740.
11. Viegas SF, Patterson RM, Hillman GR, Peterson PD, Crossley M, Foster R. Simulated scaphoid proximal pole fracture. J Hand Surg 1991;16A:495–500.
12. Herbert TJ, Fisher WE. Management of the fractured scaphoid using a new bone screw. J Bone Joint Surg 1984;66B:114–123.
13. Garcia-Elias M, Lluch A. Partial excision of scaphoid: is it ever indicated? Hand Clin 2001;17:687–695.
14. Moritomo H, Tada K, Yoshida T, Masatomi T. The relationship between the site of nonunion of the scaphoid and scaphoid nonunion advanced collapse (SNAC). J Bone Joint Surg 1999;81B: 871–876.
15. Viegas SF, Yamaguchi S, Boyd NL, Patterson RM. The dorsal ligaments of the wrist: anatomy, mechanical properties, and function. J Hand Surg 1999;24A:456–468.

SCIENTIFIC ARTICLE

Change in the Length of the Ulnocarpal Ligaments During Radiocarpal Motion: Possible Impact on Triangular Fibrocartilage Complex Foveal Tears

Hisao Moritomo, MD, PhD, Tsuyoshi Murase, MD, PhD, Sayuri Arimitsu, MD, Kunihiro Oka, MD, PhD, Hideki Yoshikawa, MD, PhD, Kazuomi Sugamoto, MD, PhD

Purpose The fovea of the ulnar head is the primary attachment site for both the distal radioulnar and the ulnocarpal ligaments. Thus, both ligaments should be simultaneously affected by the traumatic avulsion of the triangular fibrocartilage complex from its ulnar attachment. Little attention, however, has been directed toward the role of the ulnocarpal ligaments in the mechanics of this type of injury. The purpose of this study was to investigate the changes in length of the ulnocarpal ligaments during various radiocarpal motions and to determine the type of radiocarpal motion that makes the ulnocarpal ligament taut and that could cause foveal avulsion if it were excessive.

Methods The 3-dimensional kinematics of the wrist joint were investigated noninvasively using a markerless bone registration technique *in vivo*. Magnetic resonance images of the wrists of 15 healthy volunteers were acquired in at least 5 positions during each wrist flexion–extension motion, radioulnar deviation, or the so called dart-throwing motion (radial extension–ulnar flexion motion). The 3-dimensional ligament paths of the ulnotriquetral, ulnolunate, ulnocapitate, and palmar radioulnar ligaments were modeled as the shortest paths between the fovea and the insertion point of each ligament. Changes in the 3-dimensional ligament length of each ligament between the neutral position and each wrist position were then calculated.

Results The lengths of the ulnotriquetral and ulnocapitate ligaments increased the most on wrist radial extension, and the length of the ulnolunate ligament increased the most on wrist extension. The length of the palmar radioulnar ligament changed minimally during any motion.

Conclusions The ulnocarpal ligaments are likely to be stretched tensely in wrist radial extension and wrist extension. This study supports the hypothesis that one of the mechanisms responsible for a triangular fibrocartilage complex foveal tear is excessive traction of the ulnocarpal ligament caused by a fall on the outstretched hand. *(J Hand Surg 2008;33A:1278–1286.*

Key words Biomechanics, fovea, triangular fibrocartilage complex, ulnocarpal ligament, wrist.

Additional material is available online.

From the Department of Orthopaedics, Osaka University Graduate School of Medicine, Osaka, Japan.

Received for publication August 7, 2007; accepted in revised form April 30, 2008.

Supported in part by Grants-in-aid for Scientific Research, the Ministry of Education, Science, and Culture of Japan.

Corresponding author: Hisao Moritomo, MD, PhD, Department of Orthopaedics, Osaka University Graduate School of Medicine. 2-2 Yamadaoka, Suita-shi, Osaka, 565-0871, Japan; e-mail: moritomo@ort.med.osaka-u.ac.jp.

0363-5023/08/33A08-0003$34.00/0
doi:10.1016/j.jhsa.2008.04.033

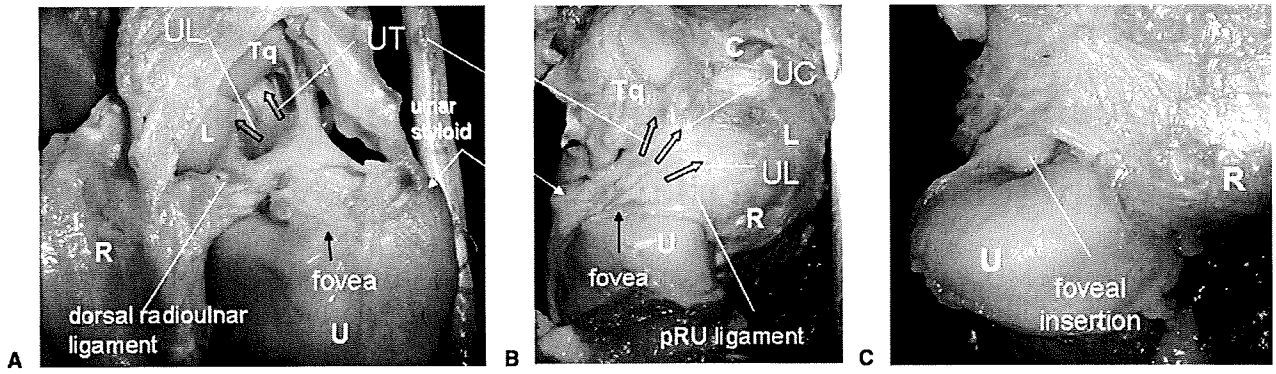

FIGURE 1: Anatomy of the ulnocarpal ligaments in a right cadaver wrist. A Dorsal view, B and C palmar views (C in supination). The ulnotriquetral (UT), ulnocapitate (UC), and ulnolunate (UL) ligaments originate together at the fovea of the ulnar head and the base of the ulnar styloid. These ligaments, along with the palmar radioulnar (pRU) ligament, extend distally like a fan in the coronal plane and insert at the palmar aspects of the triquetrum (Tq), capitate (C), and lunate (L). The joint capsule and the extensor tendons are removed. The ulnocapitate ligament is not visible from the dorsal view. R, radius; U, ulna.

THE DISTAL ULNA and the triangular fibrocartilage complex (TFCC) attached to it are essential in the coordination of the distal radioulnar joint and the ulnocarpal joint.[1] The distal radioulnar ligament and the ulnocarpal ligament are both essential ligamentous components of the TFCC. They originate together at the fovea of the ulnar head and at the base of the ulnar styloid process (Fig. 1).[1,2] A recent biomechanical study has shown that the foveal insertion has a greater effect on stability than does the styloid insertion.[3] It has been suggested that the reason for this is the closer relationship of the foveal insertion to the rotational axis of the forearm that runs through the foveal region.[4]

The foveal insertion of the TFCC is a key stabilizer of the distal radioulnar joint.[3] Thus, when this insertion fails to heal adequately after injury, distal radioulnar joint instability may develop, resulting in pain, decreased grip strength, and mechanical symptoms. Based on this concept, clinicians have recently advocated that patients with ulnar detachment of the TFCC require repair of the TFCC not to the capsule[5] but to the fovea.[6-8]

Despite the recognition of foveal lesions and their effects on distal radioulnar joint stability, the mechanism of injury in a foveal tear remains unclear. Only a few biomechanical studies have examined the mechanism of injury of the TFCC foveal tear.[9,10] It has been suggested that traumatic foveal lesions result from forces generated by forearm hyper-rotation, distal radioulnar joint distraction, wrist axial loading, or some combination of these factors.[8,11] However, neither extreme rotational forces[9] nor the axial load during injury[10] alone can reproduce a traumatic foveal lesion.

A few biomechanical investigations of the function of the ulnocarpal ligament suggest that the ulnocarpal ligament has an important role in stabilizing the ulnocarpal joint[12,13]; however, there has been little or no discussion of the relationship between the ulnocarpal ligament and the foveal triangular fibrocartilage complex tear. Moreover, all of the current information regarding the function of the ulnocarpal ligament has been acquired in cadaver model studies using invasive procedures. Such *in vitro* experiments cannot completely reproduce the physical muscular force that is exerted across the wrist joint *in vivo*. This limitation could alter the normal kinematics of the ligaments. Recently, researchers have been able to measure *in vivo* kinematics of the human joint[14-16] and ligament length[17] using noninvasive techniques.

The fovea of the ulnar head is the primary attachment site for both the distal radioulnar and ulnocarpal ligaments, so that both are affected simultaneously by traumatic avulsion of the TFCC from its ulnar attachment. We therefore designed this study to investigate changes in the length of the ulnocarpal ligaments during various radiocarpal motions using *in vivo* 3-dimensional motion analysis. The purpose of this study was to determine the type of wrist radiocarpal motion that makes the ulnocarpal ligament taut and can cause foveal avulsion if it is excessive.

MATERIALS AND METHODS

The *in vivo* 3-dimensional kinematics of the wrist joint in a total of 15 right wrists of healthy volunteers was studied. Flexion–extension motion, radioulnar deviation, and the so-called dart-throwing motion were investigated in 5 volunteers each. The average age of the volunteers was 28 years (range, 20–32 years). There were 11 men and 4 women. All volunteers gave their written informed consent prior to inclusion in the study.

Magnetic resonance images were acquired using the same method as reported previously.[14,16] To immobilize the elbow and the wrist at a specific angle during each wrist motion, a special posture device, which has a grip bar and goniometers, was used. This device has 3 motion axes, all of which cross perpendicularly at the wrist joint and enable the wrist to move along any specific plane.

Magnetic resonance images were acquired in 7 positions during flexion–extension motion from 60° extension to 60° flexion in 20° increments, in 7 positions during radioulnar deviation from 20° radial deviation to 40° ulnar deviation in 10° increments, and in 5 positions during dart-throwing motion from 40° radial deviation–extension (radial extension) to 40° ulnar deviation–flexion (ulnar flexion) in 20° increments.

The contours of each bone were mapped from the magnetic resonance volume images. The 3-dimensional surface models of the bones were constructed using a software program (Virtual Place-M; AZE, Tokyo, Japan). The kinematic variables were calculated by registering the bone in one position and then comparing it in other positions. The volume registration technique was conducted using the same software program. The ulna, the radius, and all the carpal bones except the pisiform were registered, and the motion of each bone relative to the ulna was calculated. Three-dimensional animations of the motions of the radius, the carpus, and the ligaments with respect to the fixed ulna were created by using software that was developed in our laboratory (Orthopedics Viewer; Osaka University, Osaka, Japan).

We modeled 4 ligament paths consisting of the ulnotriquetral (UT), ulnolunate (UL), ulnocapitate (UC), and palmar radioulnar (pRU) ligaments. The origin and insertion of the ligament models investigated in this study were based on information from our own cadaver dissection and previous anatomical studies.[1,2,18] These points were located by comparing anatomic information and the bony geometry on the 3-dimensional bone model.

The UT, UC, and UL ligaments originate together at the fovea of the ulnar head and at the base of the ulnar styloid process (Figs. 1 and 2). These ligaments, along with the pRU ligament, extend distally like a fan in the coronal plane and insert at the palmar aspects of the triquetrum, capitate, and lunate. The UC ligament emerges from the fovea and courses across the anterior border of the triangular fibrocartilage and attaches into the anteromedial aspect of the capitate.[18] When the ulnocarpal ligament is inspected from the palmar side on cadaver specimens, the UT, UL, and UC ligaments

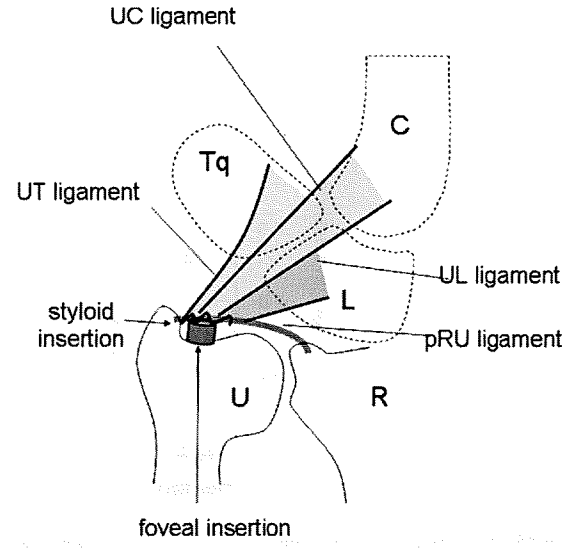

FIGURE 2: A schema of the ulnocarpal ligaments and the palmar radioulnar ligament viewed from the palmar side.

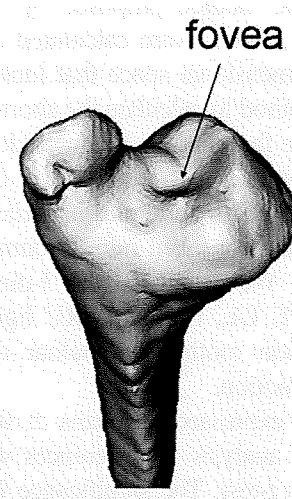

FIGURE 3: The fovea on a 3-dimensional model of the right ulna viewed from the palmar side.

are confluent but the UC ligament runs more superficial than the UT and UL ligaments. In this study, the origins of all ligaments were placed at the fovea of the ulnar head, which was determined as the deepest point of the distal surface of the ulnar head (Fig. 3).

The insertion of the UT ligament was placed at a point just ulnar to the lunotriquetral joint on the palmar tuberosity of the triquetrum. The insertion of the UL ligament was placed at a point just radial to the lunotriquetral joint on the palmar tuberosity of the lunate. The insertion of the UC ligament was placed at the proximal and ulnar corner of the palmar tuberosity of the capitate. The insertions of the pRU ligaments were placed at the ulnopalmar corner of the distal radius.

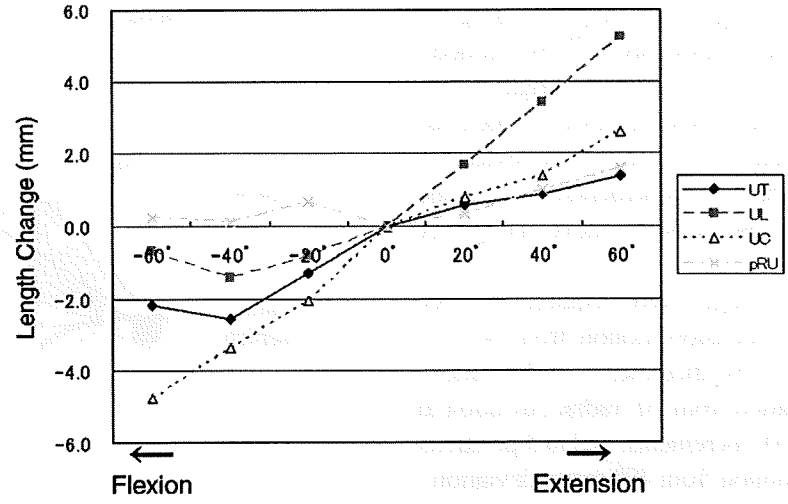

FIGURE 4: Change in the length of the 3 ulnocarpal ligaments and of the palmar radioulnar ligament during flexion–extension motion.

Based on the method proposed by Marai et al.,[17] these ligament models were calculated as the shortest paths in a 3-dimensional space that includes bone obstacles. The method to calculate the shortest paths takes into account the fact that the ligament does not go in a straight line from origin to insertion but detours around bony protrusions. Structural and material properties of the ligaments are not taken into account by this computer program. We calculated the 3-dimensional distance of the UT, UL, UC, and pRU ligaments during flexion–extension motion, radioulnar deviation, and dart-throwing motion.

All data are expressed as means ± standard deviation. Statistical analysis of differences was performed using Student's *t*-test. The significance level was $p < .05$.

RESULTS

Flexion–extension motion

From the wrist neutral position to extension, the length of the UT, UL, and UC ligaments increased by 1.4 mm ± 1.5 mm, 5.2 mm ± 1.6 mm, and 2.6 mm ± 0.5 mm, respectively (Fig. 4). From the wrist neutral position to flexion, the length of UT, UL, and UC ligaments decreased by 2.2 mm ± 1.5 mm, 0.7 mm ± 1.7 mm, and 4.8 mm ± 1.5 mm, respectively. The animations of the wrist joint from wrist flexion to extension showed that, as the triquetrum, lunate, and capitate rotate dorsally, the paths of the UT, UL, and UC ligaments gradually develop a detour toward the palmar side, because of a palmar protrusion of the proximal part of the triquetrum and lunate (Fig. 5). (The supplementary video can be viewed at the *Journal's* Web site, http://www.jhandsurg.org.) The degree of the palmar protrusion of the triquetrum in wrist extension appeared to be less than that of the lunate. The change in length of the pRU ligament was relatively small (1.6 mm ± 1.0 mm in extension, 0.2 mm ± 0.8 mm in flexion).

Radioulnar deviation

From the wrist neutral position to radial deviation, the length of the UT, UL, and UC ligaments increased by 1.1 mm ± 0.4 mm, 0.0 mm ± 0.5 mm, and 0.9 mm ± 0.8 mm, respectively (Fig. 6). From the wrist neutral position to ulnar deviation, the length of the UT and UC ligaments decreased by 1.1 mm ± 0.8 mm and 2.1 mm ± 2.0 mm, respectively, but that of the UL ligament increased by 2.3 mm ± 1.7 mm. The animations showed that, during radioulnar deviation, the UT and UC ligaments and the UL ligament showed reciprocal behavior with respect to each other (Fig. 7). (The supplementary video can be viewed at the *Journal's* Web site, http://www.jhandsurg.org.) During wrist ulnar deviation, the lunate rotated dorsally, which appeared to stretch the UL ligament. The triquetrum also rotated dorsally but shifted toward the ulnar head, which appeared to cancel the length increase of the UT ligament generated by dorsal rotation. The length of the pRU ligament changed minimally (0.3 mm ± 0.5 mm in radial deviation, 0.3 mm ± 0.3 mm in ulnar deviation).

Dart-throwing motion

From the wrist neutral position to radial extension, the length of the UT, UL, and UC ligaments increased by 3.0 mm ± 1.7 mm, 1.8 mm ± 1.7 mm, and 4.0 mm ±

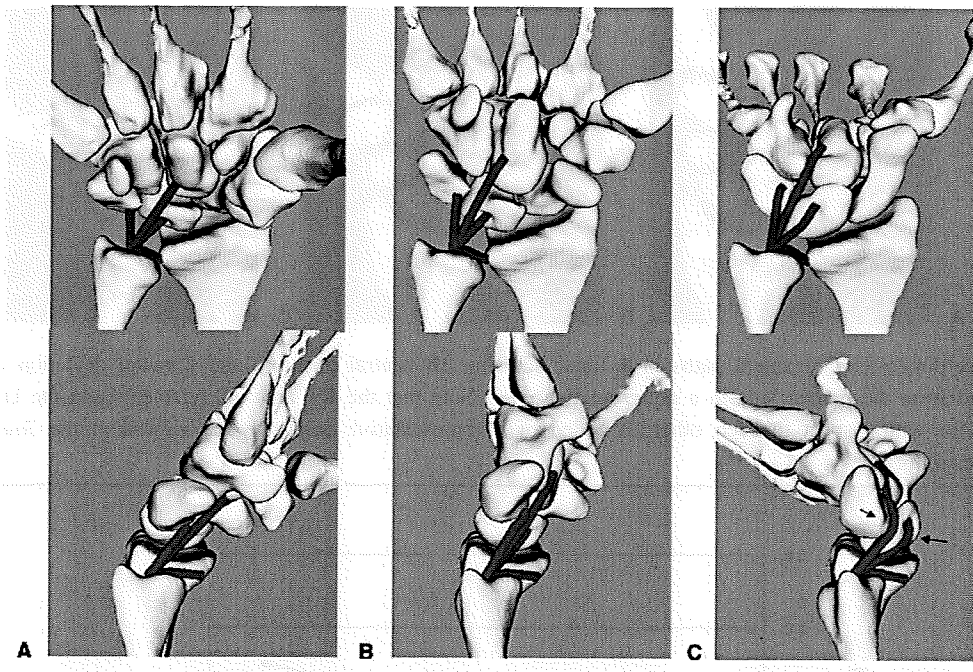

FIGURE 5: Three-dimensional ligament paths in wrist flexion **A**, neutral position **B**, and extension **C** during flexion–extension motion viewed from the palmar side and the ulnar side in a representative case. Note that, in wrist extension, the ligament paths detour toward the palmar side because of the palmar protrusion of the triquetrum and lunate (arrow). A video of a representative case may be viewed at the *Journal's* Web site, http://www.jhandsurg.org.

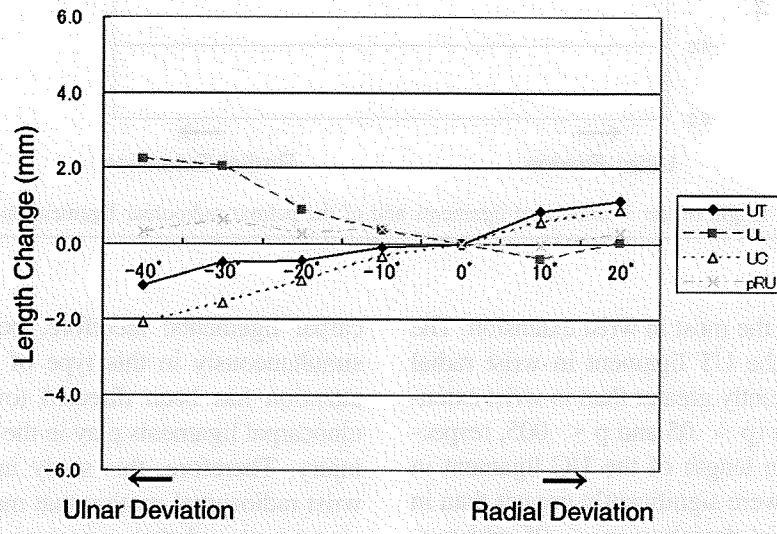

FIGURE 6: Change in the length of the 3 ulnocarpal ligaments and of the palmar radioulnar ligament during radioulnar deviation.

1.1 mm, respectively (Fig. 8). From the wrist neutral position to ulnar flexion, the length of the UT and UC ligaments decreased by 1.6 mm ± 0.5 mm and 2.2 mm ± 0.6 mm, respectively, but that of the UL ligament increased by 1.2 mm ± 1.1 mm. The animations showed that, in wrist radial extension, the capitate insertion of the UC ligament shifted to the radiodorsal direction, and palmar protrusion of the capitate head made the UC ligament detour toward the palmar side (Fig. 9). (The supplementary video can be viewed at the *Journal's* Web site, http://www.jhandsurg.org.) The animations also showed that the triquetrum shifted distally, whereas the lunate moved only slightly. The length of the pRU ligament changed little (0.5 mm ± 1.0 mm in radial extension, 1.2 mm ± 0.6 mm in ulnar flexion).

The length of the UT and UC ligaments increased the most in wrist radial extension, and the length of the

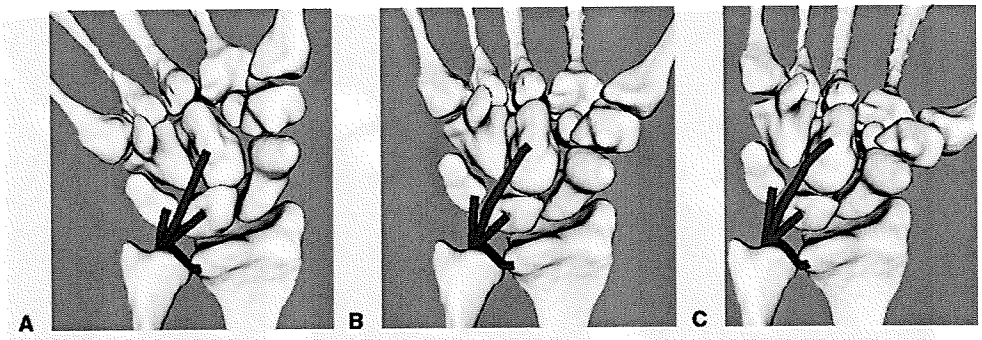

FIGURE 7: Three-dimensional ligament paths in **A** ulnar deviation, **B** neutral position, and **C** radial deviation during radioulnar deviation, viewed from the palmar side in a representative case. Note that the UT and UC ligaments and the UL ligament show reciprocal behavior with respect to each other. A video of a representative case may be viewed at the *Journal's* Web site, http://www.jhandsurg.org.

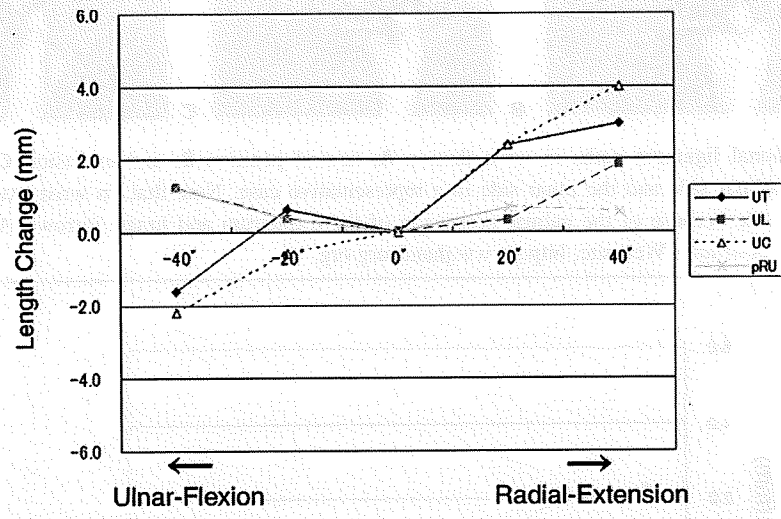

FIGURE 8: Change in the length of the 3 ulnocarpal ligaments and of the palmar radioulnar ligament during dart-throwing motion.

UL ligament increased the most in wrist extension. The changes in length of the UT ligament in wrist radial extension were significantly greater than in wrist extension or radial deviation ($p < .05$ and $p < .005$, respectively). The changes in length of the UC ligament in wrist radial extension were significantly greater than in wrist extension or radial deviation ($p < .05$ and $p < .005$, respectively). The changes in length of the UL ligament in wrist extension were significantly greater than in wrist radial extension ($p < .05$). The length of the pRU ligament did not change significantly in any motion.

DISCUSSION

The pathomechanics of a traumatic triangular fibrocartilage complex foveal tear are not yet well understood. Anatomically, the fovea of the ulnar head is the primary attachment site for both the distal radioulnar and ulnocarpal ligaments; therefore, both should be affected simultaneously in this type of injury. However, little attention has been directed toward the role that the ulnocarpal ligaments play in the pathomechanics of this injury. Therefore, this study investigated the type of wrist radiocarpal motion that makes the ulnocarpal ligament taut and that can cause foveal avulsion of the TFCC if the motion is excessive.

The present *in vivo* study has some limitations. The origin and insertion of the ligaments were determined based only on anatomic information; individual variances in ligamentous anatomy were not taken into account. Our method does not take into account the width or the material properties of the ligaments. Real ligaments seldom extend or contract, although in our videos the ligament models appear elastic (Videos may be viewed at the *Journal's* Web site, www.jhandsurg.org.). This fact may influence the interaction with

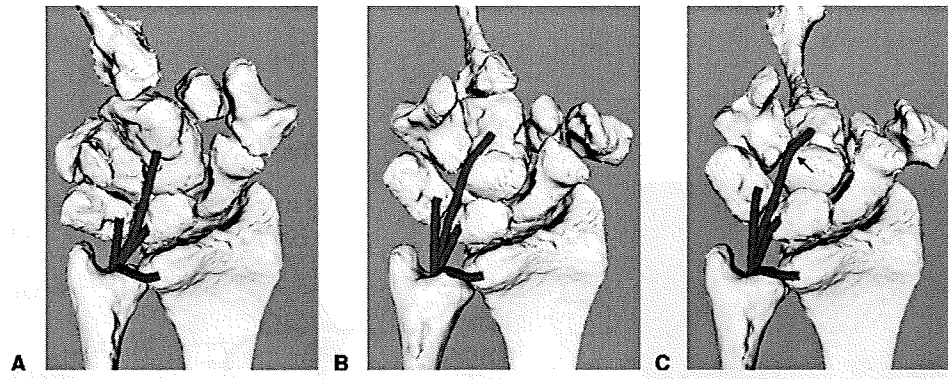

FIGURE 9: Three-dimensional ligament paths in **A** flexion, **B** neutral position, and **C** extension during dart-throwing motion, viewed from the palmar side in a representative case. The third metacarpals are shown, to indicate the global wrist position. Note that the capitate insertion of the UC ligament shifted to the radiodorsal direction, and palmar protrusion of the capitate head made the UC ligament detour toward the palmar side. A video of a representative case can be viewed at the *Journal's* Web site, http://www.jhandsurg.org.

neighboring soft tissues, such as the adjacent ligaments, the articular disk, and the meniscus homolog. Nonetheless, the animations of the ulnocarpal ligament paths that were created provided new visual information about the ligamentous kinematics and helped identify a potential mechanism for TFCC foveal tear.

There has been some confusion regarding the origin of the ulnocarpal ligament. When the ulnocarpal ligaments are inspected arthroscopically, their origin appears to be along the entire palmar extent of the triangular fibrocartilage complex. When inspected from the palmar side on cadaver specimens, however, the 3 fibers of the ulnocarpal ligaments are confluent and appear to converge into the fovea. We think that the ulnocarpal ligament that is seen arthroscopically is just a distal part of the ligaments, and that in fact the fibers of these ligaments extend proximally toward the fovea—although some fibers of the ligaments mingle with the palmar radioulnar ligament.

The function of the ulnocarpal ligament is not yet fully understood.[18,19] In particular, the ligamentous behavior during the dart-throwing motion has never been investigated. Weaver et al.[20] investigated the *in situ* tensions of the UL ligament in cadaver specimens and found that the tension of the UL ligament increased in ulnar deviation, supination, and extension. Wiesner et al.[21] applied progressive posteroanterior forces in the palmar direction to the carpus and found that the largest displacement was observed after the ulnar insertion of the ulnocarpal ligaments was sectioned. It has also been reported that the ulnocarpal ligaments can prevent abnormal radioulnar translations of the carpus.[12,13] All these findings suggest that the ulnocarpal ligaments have an important role in stabilizing the ulnocarpal joint.

We found that the greatest length increase of the UT and UC ligaments occurred with wrist radial extension during dart-throwing motion. It has been reported that midcarpal motion is substantial during dart-throwing motion,[16] and that the scaphoid and lunate move less.[15] Our animations in wrist radial extension showed that the capitate insertion of the UC ligament shifted distally, and that the UC ligament path developed a detour due to the palmar protrusion of the capitate head. The animations also showed that the triquetrum shifted distally without significant rotation, while the lunate seldom moved. These carpal movements that occur during wrist hyper-radial extension motion result in substantial strain to the UC and UT ligaments and on the foveal insertion of the TFCC. In comparison, the greatest length increase of the UL ligament was found in pure wrist extension. In the wrist extension animation, the palmar protrusion of the proximal portion of the lunate was greater than that of the triquetrum. This may explain why the length of the UL ligament increased more than the length of the UT ligament. In wrist extension, the UL ligament probably becomes taut and stretches the foveal insertion of the TFCC as well.

From wrist ulnar deviation to radial deviation, the length of the UT ligament increased, but the length of the UL ligament decreased. That is, during radioulnar deviation, the UT ligament and the UL ligament showed reciprocal behavior with respect to each other. We note that these 2 ligaments have an opposite function in terms of carpal stability during radioulnar deviation, even though, macroscopically, these 2 ligaments are often confluent and indistinguishable from each

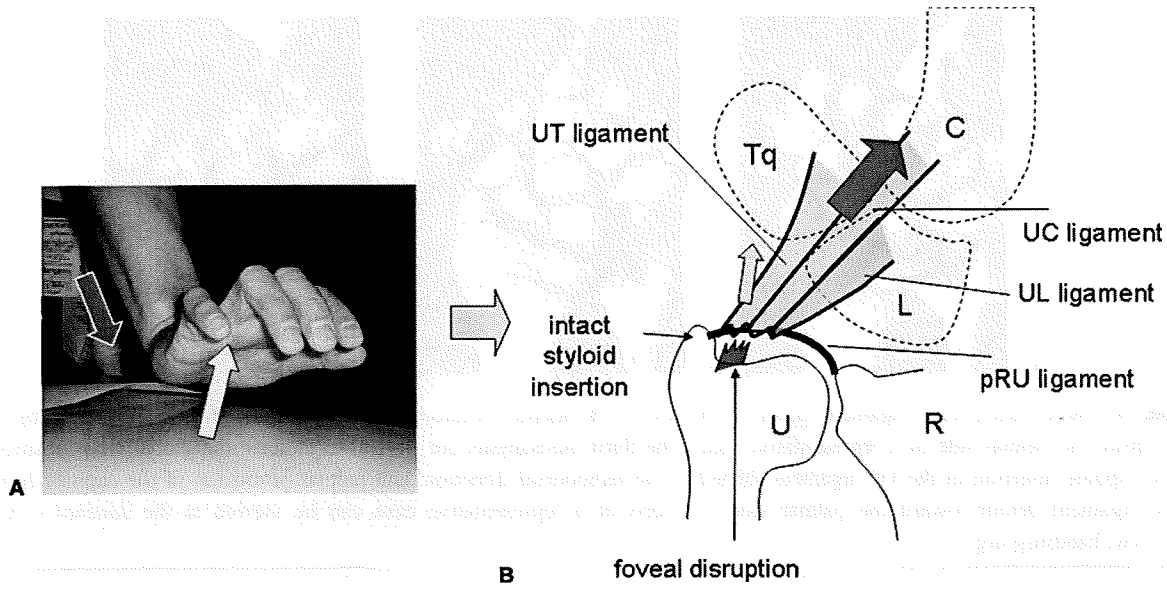

FIGURE 10: A Foveal disruption can result from a fall on the outstretched hand due to excessive traction of the ulnocarpal ligament in hyper-radial extension or extension of the wrist. The styloid insertion may be left intact. **B** The hypothesized mechanism of a triangular fibrocartilage complex foveal tear.

other.[18] It is possible that these 2 ligaments work together to provide a continuous and stable ulnar–radial–carpal motion throughout wrist radioulnar deviation.

The visualization of the pathomechanics of the TFCC tear may have been obscured by the relatively rigid prominence given to rotational injuries of the forearm; in fact, almost half of the reported cases of triangular fibrocartilage complex tears result from a fall on the outstretched hand.[6,7,22,23] For example, Hermansdorfer and Kleinman[6] reported 11 cases of peripheral triangular fibrocartilage complex tears, which included 5 cases caused by a fall. These facts strongly imply that forced wrist extension or radial extension, rather than forced pronosupination, may be a major factor in the pathomechanics of this type of injury (Fig. 10).

Based on the present findings, one possible injury mechanism of a triangular fibrocartilage complex foveal tear is excessive traction of the ulnocarpal ligament caused by wrist hyper-radial extension or hyperextension. However, this lesion does not result from forces generated only by simple wrist hyper-radial extension or hyperextension. Additional forces, such as axial loading or forearm rotation (or both), are probably required, at least to initiate the tear. Considering that the ulnocarpal ligament has another origin on the palmar aspect of the ulnar styloid,[2] which is eccentric from the center of forearm rotation (fovea), it is easily seen that the change in length of this fascicle would be increased by forearm supination. Strain of this fascicle during forearm supination may thus affect the tension of the foveal insertion.

This biomechanical study supports the hypothesis that one of the mechanisms of TFCC foveal tear can be excessive traction of the ulnocarpal ligament caused by a fall on the outstretched hand. Thus, to identify the exact location of the TFCC tear, clinical and radiographic examinations that pay particular attention to the ulnocarpal ligament lesion should be considered when dealing with patients who have ulnar wrist pain.

REFERENCES

1. Hagert CG. Current concepts of the functional anatomy of the distal radioulnar joint, including the ulnocarpal junction. In: Büchler U, ed. Wrist instability. London: Martin Dunitz, 1996:15–21.
2. Ishii S, Palmer AK, Werner FW, Short WH, Fortino MD. An anatomic study of the ligamentous structure of the triangular fibrocartilage complex. J Hand Surg 1998;23A:977–985.
3. Haugstvedt JR, Berger RA, Nakamura T, Neale P, Berglund L, An KN. Relative contributions of the ulnar attachments of the triangular fibrocartilage complex to the dynamic stability of the distal radioulnar joint. J Hand Surg 2006;31A:445–451.
4. Hagert CG. Distal radius fracture and the distal radioulnar joint: anatomical considerations. Handchir Mikrochir Plast Chir 1994;26: 22–26.
5. Trumble TE, Gilbert M, Vedder N. Isolated tears of the triangular fibrocartilage: management by early arthroscopic repair. J Hand Surg 1997;22A:57–65.
6. Hermansdorfer JD, Kleinman WB. Management of chronic peripheral tears of the triangular fibrocartilage complex. J Hand Surg 1991;16A:340–346.
7. Sennwald GR, Lauterburg M, Zdravkovic V. A new technique of reattachment after traumatic avulsion of the TFCC at its ulnar insertion. J Hand Surg 1995;20B:178–184.
8. Adams BD, Berger RA. An anatomic reconstruction of the distal

radioulnar ligaments for posttraumatic distal radioulnar joint instability. J Hand Surg 2002;27A:243–251.
9. Heiple KG, Freehafer AA, Van't Hof A. Isolated traumatic dislocation of the distal end of the ulna or distal radio-ulnar joint. J Bone Joint Surg 1962;44A:1387–1394.
10. Adams BD, Samani JE, Holley KA. Triangular fibrocartilage injury: a laboratory model. J Hand Surg 1996;21A:189–193.
11. Palmer AK. Triangular fibrocartilage complex lesions: a classification. J Hand Surg 1989;14A:594–606.
12. Yin Y, Mann FA, Hodge JC, Gilula LA. Roentgenographic interpretation of ligamentous instabilities of the wrist. In: Gilula LA, Yin Y, eds. Imaging of the wrist and hand. Philadelphia: WB Saunders, 1996:203–224.
13. Allieu Y, Garcia-Elias M. Dynamic radial translation instability of the carpus. J Hand Surg 2000;25B:33–37.
14. Goto A, Moritomo H, Murase T, Oka K, Sugamoto K, Arimura T, et al. In vivo three-dimensional wrist motion analysis using magnetic resonance imaging and volume-based registration. J Orthop Res 2005;23:750–756.
15. Crisco JJ, Coburn JC, Moore DC, Akelman E, Weiss AP, Wolfe SW. In vivo radiocarpal kinematics and the dart thrower's motion. J Bone Joint Surg 2005;87A:2729–2740.
16. Moritomo H, Murase T, Goto A, Oka K, Sugamoto K, Yoshikawa H. In vivo, three-dimensional kinematics of the midcarpal joint of the wrist. J Bone Joint Surg 2006;88A:611–621.
17. Marai GE, Laidlaw DH, Demiralp C, Andrews S, Grimm CM, Crisco JJ. Estimating joint contact areas and ligament lengths from bone kinematics and surfaces. IEEE Trans Biomed Eng 2004;51: 790–799.
18. Garcia-Elias M. Soft-tissue anatomy and relationships about the distal ulna. Hand Clin 1998;14:165–176.
19. Ritt MJ, Stuart PR, Berglund LJ, Linscheid RL, Cooney WP III, An KN. Rotational stability of the carpus relative to the forearm. J Hand Surg 1995;20A:305–311.
20. Weaver L, Tencer AF, Trumble TE. Tensions in the palmar ligaments of the wrist. I. The normal wrist. J Hand Surg 1994;19A:464–474.
21. Wiesner L, Rumelhart C, Pham E, Comtet JJ. Experimentally induced ulno-carpal instability: a study on 13 cadaver wrists. J Hand Surg 1996;21B:24–29.
22. Cooney WP, Linscheid RL, Dobyns JH. Triangular fibrocartilage tears. J Hand Surg 1994;19A:143–154.
23. Mikic ZD. Treatment of acute injuries of the triangular fibrocartilage complex associated with distal radioulnar joint instability. J Hand Surg 1995;20A:319–323.